Dalton Transactions

ROYAL SOCIETY OF CHEMISTRY

PAPER

Check for updates

Cite this: *Dalton Trans.*, 2021, **50**, 13915

Manganese and iron PCP pincer complexes – the influence of sterics on structure and reactivity†

Wolfgang Eder, [a] Daniel Himmelbauer, [a] Berthold Stöger, [b] Luis F. Veiros, [c] Marc Pignitter [d] and Karl Kirchner *[a]

Received 20th July 2021,
Accepted 5th September 2021

DOI: 10.1039/d1dt02407h

rsc.li/dalton

The syntheses of various manganese and iron PCP pincer complexes *via* a solvothermal oxidative addition methodology is described. Upon reacting $[Mn_2(CO)_{10}]$ with the ligands (P(C–Br)P^{CH_2}-iPr) (**1a**) and (P(C–Br)P^{O}-iPr) (**1b**), Mn(I) PCP pincer complexes $[Mn(PCP^{CH_2}\text{-iPr})(CO)_3]$ (**2a**) and $[Mn(\text{-}PCP^{O}\text{-iPr})(CO)_3]$ (**2b**) were obtained. Protonation of **2a** with $HBF_4{\cdot}Et_2O$ led to the formation of $[Mn(\kappa^3P,CH,P\text{-}P(CH)P^{CH_2}\text{-iPr})(CO)_3]BF_4$ (**3**) featuring an η^2-C_{aryl}–H agostic bond. The solvothermal reaction of **1a** with $[Fe_2(CO)_9]$ afforded the Fe(II) PCP pincer complex $[Fe(PCP^{CH_2}\text{-iPr})(CO)_2Br]$ (**4**). Treatment of **4** with $Li[HBEt_3]$ afforded the Fe(I) complex $[Fe(PCP^{CH_2}\text{-iPr})(CO)_2]$ (**5a**). When using the sterically more demanding ligands (P(C–Br)P^{CH_2}-*t*Bu) (**1c**) and (P(C–Br)P^{O}-*t*Bu)(**1d**) striking differences in reactivity were observed. While neither **1c** nor **1d** showed any reactivity towards $[Mn_2(CO)_{10}]$, the reaction with $[Fe_2(CO)_9]$ and $[Fe(CO)_5]$ led to the formation of the Fe(I) complexes $[Fe(PCP^{CH_2}\text{-}t\text{Bu})(CO)_2]$ (**5b**) and $[Fe(PCP^{O}\text{-}t\text{Bu})(CO)_2]$ (**5c**). X-ray structures of representative complexes are provided.

Introduction

Pincer complexes[1] have received considerable attention in the last decades.[2] Their high stability in addition to their facile modifiability make them attractive compounds in transition metal chemistry as well as for the examination of stoichiometric and catalytic reactions.[2] In particular PCP pincer complexes consisting of a benzene backbone onto which phosphine donors are attached *via* O, NR or CH_2 linkers, first introduced in 1976,[3] are a very interesting class of compounds. As far as first row transition metals are concerned, the chemistry of these complexes is, with the exception of nickel, not very comprehensive. Indeed, reports of PCP complexes of iron and especially manganese are exceedingly rare.[4–8] A reason for the lack of base metal PCP pincer complexes is that many metal precursors are low-valent carbonyl compounds which fail to activate the arene C–H bond primarily for thermodynamic reasons due to the instability of the resulting hydride complexes. Recently, it was shown that oxidative addition of P(C–X)P (X = Cl, Br) ligands onto low valent base metal precursors can be used to gain entry into base metal PCP pincer chemistry.[7–11]

In this paper, the oxidative addition of the C–Br bond of the ligand precursors P(C–Br)P^{CH_2}-R and P(C–Br)P^{O}-R (R = iPr, *t*Bu) to the Mn(0) and Fe(0) complexes $[Mn_2(CO)_{10}]$ and $[Fe_2(CO)_9]$ was utilized to synthesize, characterize and study the reactivity of Mn(I), Fe(I) and Fe(II) PCP pincer complexes. Striking differences in the reactivity between the ligands with iPr moieties attached to the phosphorus donor atom and their corresponding sterically more demanding *t*Bu analogues were observed. Moreover, also differences between pincers featuring O, NR or CH_2 linkers are significant. X-ray structures of the new complexes are presented.

Results and discussion

Manganese PCP pincer complexes

The Mn(0) complex $[Mn_2(CO)_{10}]$ and 2 equiv. of (P(C–Br)P^{CH_2}-iPr) (**1a**) were dissolved in CH_3CN and reacted under solvothermal conditions for 18 h at 150 °C. Workup of the resulting orange solution *via* column chromatography afforded the diamagnetic, air-stable, tricarbonyl Mn(I) complex $[Mn(PCP^{CH_2}\text{-iPr})(CO)_3]$ (**2a**) in 31% isolated yield (Scheme 1). The reaction formally constitutes a one electron oxidation of the Mn center, with the ligand **1a** acting as the oxidant. Similarly, under the same conditions, the reaction of the POCOP-ligand (P(C–Br)

[a]*Institute of Applied Synthetic Chemistry, Vienna University of Technology, Getreidemarkt 9, A-1060 Vienna, Austria. E-mail: karl.kirchner@tuwien.ac.at*
[b]*X-Ray Center, Vienna University of Technology, Getreidemarkt 9, A-1060 Vienna, Austria*
[c]*Centro de Química Estrutural, Instituto Superior Técnico, Universidade de Lisboa, Av. Rovisco Pais No. 1, 1049-001 Lisboa, Portugal*
[d]*Department of Physiological Chemistry, Faculty of Chemistry, University of Vienna, Althanstrasse 14, 1090 Vienna, Austria*

†Electronic supplementary information (ESI) available: Complete crystallographic data and technical details in CIF format for **2a**, **3**, **4**, **5b** and **5c**. CCDC 2097016–2097020. For ESI and crystallographic data in CIF or other electronic format see DOI: 10.1039/d1dt02407h

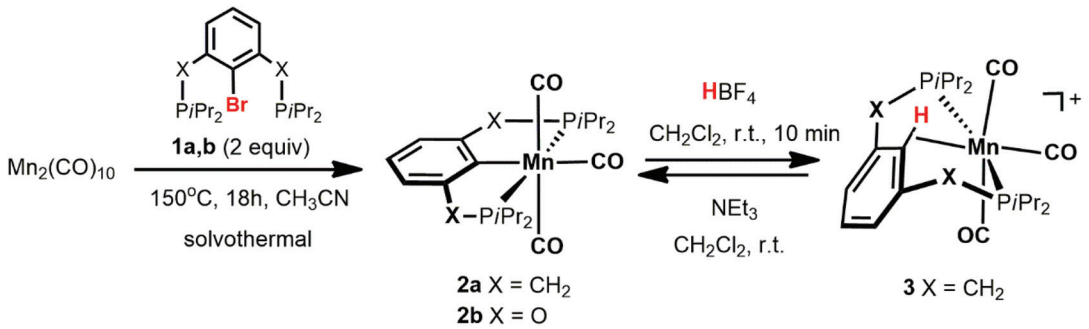

Scheme 1 Synthesis of complexes **2** and **3**.

P^{O}-iPr) (**1b**) also afforded the tricarbonyl Mn(I) complex [Mn(PCP^{O}-iPr)(CO)$_3$] (**2b**) in 39% yield, which crystallized directly from the reaction mixture after cooling to room temperature (Scheme 1). In both cases, the fate of the bromine and the remaining Mn fragments could not be established.

Complexes **2a** and **2b** were fully characterized by a combination of ^{1}H, ^{13}C{^{1}H}, and ^{31}P{^{1}H} NMR spectroscopy, IR spectroscopy, and HR-MS analysis as well as single crystal X-ray diffraction in the case of **2a**. In the ^{31}P{^{1}H} NMR spectrum the complexes exhibit characteristic singlet resonances at 100.3 and 220.9 ppm for **2a** and **2b**, respectively. The carbonyl ligands of the complexes were detected as poorly resolved triplets at 223.7 ppm for **2a** and 220.1 ppm for **2b**, corresponding to the carbonyl located *trans*-to the *ipso* carbon of the pincer ligand, as well as broad resonances at 226.7 ppm (**2a**) and 222.0 ppm (**2b**), assignable to the carbonyls *cis* to the *ipso* carbon. The signals of the *ipso* carbons were detected as triplets at 173.0 (J_{CP} = 8.2 Hz) (**2a**) and 135.6 ppm (J_{CP} = 14.3 Hz) (**2b**), respectively. The IR spectra of both complexes showed characteristic bands corresponding to a *mer* arrangement of the carbonyl ligands at 1985, 1892 and 1873 cm^{-1} for **2a** and 2010, 1994 and 1984 cm^{-1} for **2b**. In addition to the spectroscopic characterization, the solid-state structure of **2a** was determined by single-crystal X-ray diffraction.

A structural view of **2a** is depicted in Fig. 1 with selected bond distances given in the captions. The coordination geometries around the manganese center corresponds to a distorted octahedron. In particular the P–Mn–P angles deviate significantly from 180° being 162.33(1)°. The C$_{ipso}$–Mn bond lengths is 2.093(1) Å.

In analogy to [Mn(PCP^{NEt}-iPr)(CO)$_3$] reported previously,[10] protonation of [Mn(PCP^{CH_2}-iPr)(CO)$_3$] (**2a**) with HBF$_4$·Et$_2$O leads to the formation of the cationic Mn(I) complex [Mn(κ^3*P*,*CH*,*P*-P(CH)P^{CH_2}-iPr)(CO)$_3$]BF$_4$ (**3**) featuring an η^2-C$_{aryl}$–H agostic bond in 86% isolated yield (Scheme 1). The agostic proton is comparatively acidic and the starting material **2a** can be recovered upon deprotonation with even relatively weak bases such as NEt$_3$. Accordingly, protonation of **2a** is fully reversible (Scheme 1). On the other hand, all attempts to protonate [Mn(PCP^{O}-iPr)(CO)$_3$] (**2b**) led to the formation of several intractable materials possibly due to P–O bond cleavage in the presence of a strong acid.

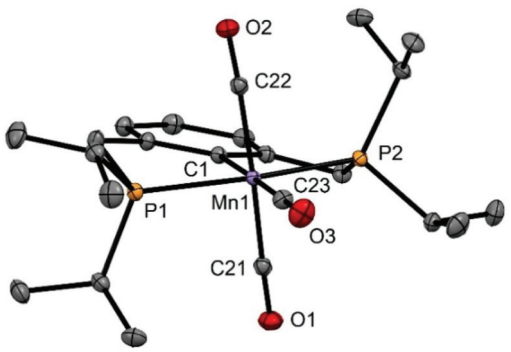

Fig. 1 Structural view of [Mn(PCP^{CH_2}-iPr)(CO)$_3$] (**2a**) showing 50% thermal ellipsoids (H atoms omitted for clarity). Selected bond lengths (Å) and bond angles (°): Mn1–C1 2.093(1), Mn1–C23 1.800(1), Mn1–C21 1.822(1), Mn1–C22 1.823(1), Mn1–P1 2.2794(4), Mn1–P2 2.772(4), P1–Mn1–P2 162.33(1), C1–Mn1–C23 178.70(4), C21–Mn1–C22 172.25(4).

Complex **3** was characterized by a combination of ^{1}H, ^{13}C{^{1}H}, and ^{31}P{^{1}H} NMR spectroscopy as well as IR, HR-MS, and X-ray crystallography. In the ^{1}H NMR spectrum a high-field shift of the proton attached to the *ipso*-carbon giving rise to a signal at 4.05 ppm can be observed. This shift is less pronounced than in the previously published NEt linked complex [Mn(κ^3*P*,*CH*,*P*-P(CH)P^{NEt}-iPr)(CO)$_3$]BF$_4$, where the agostic proton was detected at 1.36 ppm.[10] In the ^{13}C{^{1}H} NMR spectrum the *ipso*-carbon atom exhibits a signal at 84.3 ppm (*cf.* 173.0 ppm in **2a**), the three CO ligands give rise to a broad low-field resonance at 226.0 ppm and a triplet at 216.7 ppm. The relatively low $^1J_{HC}$ coupling constant of 139.1 Hz (*cf.* 126.6 Hz in [Mn(κ^3*P*,*CH*,*P*-P(CH)P^{NEt}-iPr)(CO)$_3$]BF$_4$),[8] as compared to 162.2 and 164.2 Hz for the other two aromatic C–H bonds is also typical for a strong C–H metal interaction.[13–21] Complex **3** also exhibits three strong bands at 2043, 1958, and 1911 cm^{-1} in the IR spectrum, consistent with a *mer* configuration of the carbonyls.

Structural views of **3** and, for comparison, the previously reported complex [Mn(κ^3*P*,*CH*,*P*-P(CH)P^{NEt}-iPr)(CO)$_3$]BF$_4$,[8] are shown in Fig. 2. Complex **3** features a distorted octahedral geometry around the Mn center. The distance between the *ipso*-carbon and the Mn atom is extremely long (2.408(3) Å), when compared to the Mn–C$_{ipso}$ bond distance of 2.249(2) Å in

 This journal is © The Royal Society of Chemistry 2021

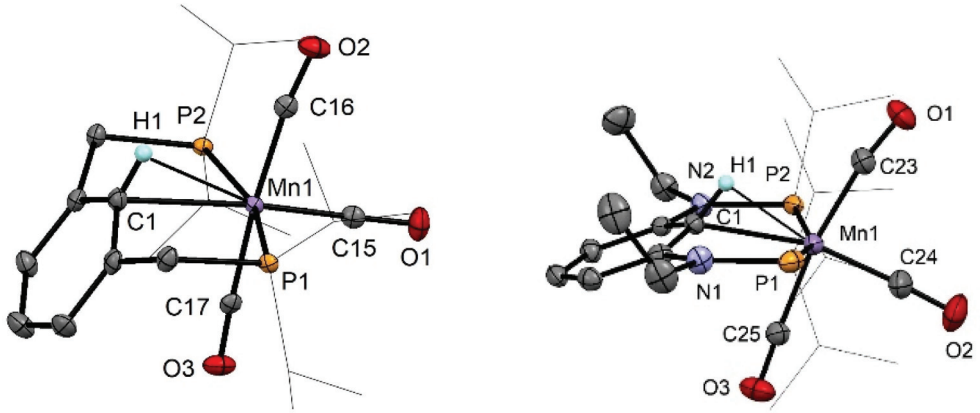

Fig. 2 Structural views of [Mn(κ^3*P,CH,P*-P(CH)P^{CH_2}-iPr)$(CO)_3$]BF_4 (**3**) (left) and [Mn(κ^3*P,CH,P*-P(CH)P^{NEt}-iPr)$(CO)_3$]BF_4 (right) showing 50% thermal ellipsoids (most H atoms and BF_4^- anion omitted for clarity). Selected bond lengths (Å) and bond angles (°) for **3**: Mn1–C1 2.408(3), Mn1–C15 1.767(3), Mn1–C16 1.851(3), Mn1–C17 1.846(3), Mn1–P1 2.3331(8), Mn1–P2 2.3334(9), Mn1–H1 2.29(3), C1–H1 0.96(3), P1–Mn1–P2 163.96(4), C16–Mn1–C17 174.7(1), C1–Mn1–C15 175.3(1). For [Mn(κ^3*P,C-H,P*-P(CH)P^{NEt}-iPr)$(CO)_3$]BF_4: Mn1–C1 2.249(2), Mn1–C24 1.789(2), Mn1–C23 1.839(2), Mn1–C25 1.845(2), Mn1–P2 2.3142(8), Mn1–P1 2.3147(7), Mn1–H1 1.99(3), C1–H1 0.97(3), P1–Mn1–P2 157.74(2), C23–Mn1–C25 171.01(9), C1–Mn1–C24 164.67(9).

[Mn(κ^3*P,CH,P*-P(CH)P^{NEt}-iPr)$(CO)_3$]BF_4. As already evident from ^{1}H NMR spectrum of **3**, the H(1) atom (which was located in difference Fourier maps and refined freely) interacts with the Mn center (2.29(3) Å). It is noteworthy that this hydrogen atom is hardly removed from the aromatic plane (*ca.* 11°) while in [Mn(κ^3*P,CH,P*-PCP^{NEt}-iPr)$(CO)_3$]BF_4 this angle is as large as 31°. The C1–H1 bond lengths of 0.96(3) Å is in the range observed in X-ray diffraction measurements for not activated hydrocarbons (*e.g.*, 1.08 Å in C_6H_6). Given these data it can be assumed that the η^2-C_{aryl}–H agostic bond of **3** is weaker as compared to the analogous NEt linked complex [Mn(κ^3*P,CH,P*-P(CH)P^{NEt}-iPr)$(CO)_3$]BF_4.

The electronic structure of **3** has been investigated by DFT calculations. The pattern obtained is typical of a low-spin d^6 metal complex with a distorted octahedral geometry, with three filled orbitals based on metal *xy*, *xz* and *yz*, corresponding to the t_{2g} set of an octahedron, and two empty e_g orbitals, with strong participation of metal z^2 and $x^2 - y^2$, respectively. There are significant Mn–C and Mn–H interactions with distances of 2.52 and 2.47 Å, respectively, and Wiberg indices of 0.10 and 0.01, by the same order. The C–H bond also reflects the agostic interaction being weaker (WI = 0.87) than the other C_{aryl}–H bonds (WI = 0.90). The agostic interaction is significantly weaker in the case of the complex with CH_2 linkers when compared to the complexes with NEt linkers: WI (Mn–C) = 0.20 and WI(Mn–H) = 0.05. This is also apparent in the C–H bond that is as weaker as the agostic interaction is stronger: d(C–H) agostic = 1.11 Å, WI = 0.76; other C(aryl)–H bonds: *d* = 1.08–1.09 A, WI = 0.90 as well as by a more negative Mn atom and a more positive PCP ligand. PCP ligands with NEt linkers are both better donors than the one with CH_2 linker: C(Mn) = −0.61 (CH_2), −0.76 (NEt), C(PCP) = 1.07 (CH_2), 1.18 (NEt) based on the NPA charges.

Interestingly, when conducting the solvothermal reaction of $[Mn_2(CO)_{10}]$ in acetonitrile with the sterically more demanding ligands PCP (P(C–Br)P^{CH_2}-*t*Bu) (**1c**) and (P(C–Br)P^{O}-^{t}Bu) (**1d**), no conversion to a PCP complex was observed and only the unreacted ligands were recovered from the reaction mixtures.

Iron PCP pincer complexes

The solvothermal reaction of $[Fe_2(CO)_9]$ with [P(C–Br)P^{CH_2}-iPr] (**1a**) in toluene at 140 °C yielded after 16 h the iron dicarbonyl complex [Fe(PCP^{CH_2}-iPr)$(CO)_2$Br] (**4**) in 58% isolated yield (Scheme 2). The complex was fully characterized by a combi-

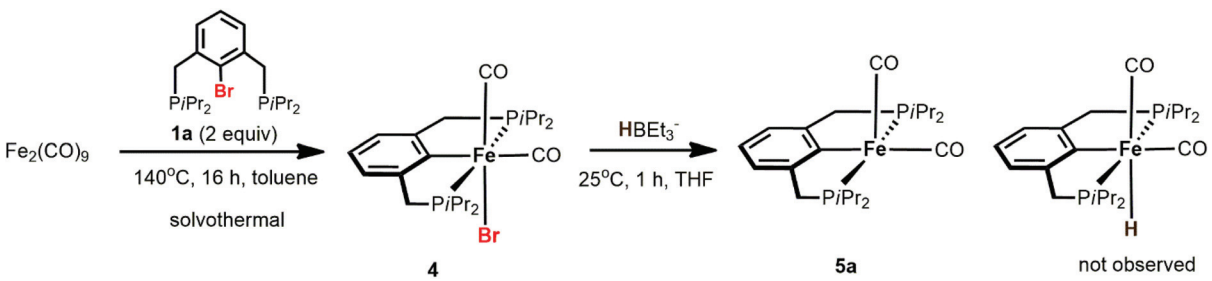

Scheme 2 Synthesis of complexes **4** and **5a**.

nation of ^{1}H, $^{13}C\{^{1}H\}$, and $^{31}P\{^{1}H\}$ NMR spectroscopy, IR spectroscopy, and HR-MS analysis. The $^{13}C\{^{1}H\}$ NMR shows two characteristic triplet low field triplet resonances at 218.1 ppm (J_{PC} = 25.2 Hz) and 213.0 ppm (J_{PC} = 12.7 Hz) that can be assigned to the carbonyl ligands. The *ipso* carbon was detected at 170.6 ppm (J_{PC} = 15.2 Hz). The $^{31}P\{^{1}H\}$ NMR spectrum shows a singlet resonance at 88.4 ppm. In the IR spectrum, the complex shows two strong absorption bands at 1993 and 1938 cm^{-1} indicating a *cis* arrangement of the CO ligands. The spectroscopic data are in good agreement with a related xylenol-based pincer complex published by Dauth *et al.*[6] The structure of **4** was also elucidated by means of single-crystal X-ray crystallography. A molecular view is depicted in Fig. 3 with selected bond lengths and angles reported in the caption. This complex adopts a slightly distorted octahedral geometry with an Fe–C bond length of 2.036(4) Å.

Complex **4** was treated with 1 equiv. of Li[$HBEt_3$] in an effort to generate the hydride complex [Fe(PCP^{CH_2}-iPr)$(CO)_2$H]. However, in analogy to the complex [Fe(PCP^{NEt}-iPr)$(CO)_2$Cl] reported previously,[7] a formal one electron reduction of the complex was observed and the green air-sensitive Fe(I) complex [Fe(PCP^{CH_2}-iPr)$(CO)_2$] (**5a**) was isolated in 80% yield (Scheme 3). A similar reaction was reported by Thompson *et al.* with the PNP pyrrole-based complex and [Fe(^{Cy}PNP)Cl$(CO)_2$], which upon treatment with Na[$HBEt_3$] yielded the Fe(I) complex [Fe(^{Cy}PNP)$(CO)_2$].[22]

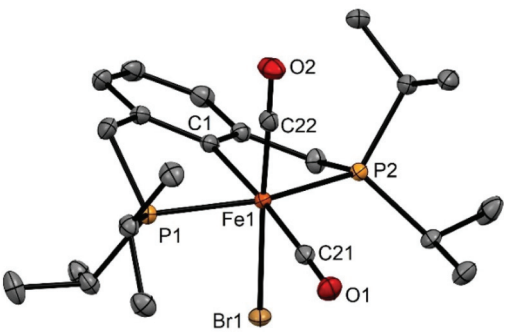

Fig. 3 Crystal Structure of [Fe(PCP^{CH_2}-*t*Bu)$(CO)_2$] (**4**) with 50% thermal ellipsoids (H atoms omitted for clarity). Selected bond lengths (Å) and bond angles (°): Fe1–C1 2.036(2), Fe1–C21 1.805(2), Fe1–C22 1.738(129), Fe1–Br1 2.5209(3), Fe1–P1 2.2602(5), Fe1–P2 2.2731(5), P1–Fe1–P2 160.69(2), C1–Fe1–C21 176.28(7), Br1–Fe1–C22 177.40(6).

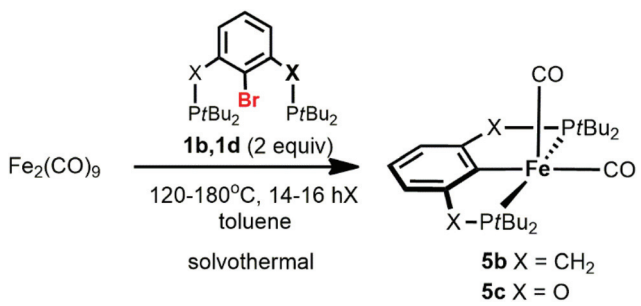

Scheme 3 Synthesis of complexes **5b** and **5c**.

Electron paramagnetic resonance (EPR) studies and solution magnetic susceptibility measurements (benzene, Evans method) were performed. The solution effective magnetic moment of 1.7(8)μ_B is in agreement with a low-spin d^7 center (one unpaired electron). X-band EPR studies were conducted in toluene glass at 100 K showing a rhombic spectrum with simulated anisotropic *g* values of g_x = 2.075, g_y = 2.045 and g_z = 2.005 with well resolved hyperfine coupling (A_x = 13.98 G, A_y = 15.44 G and A_z = 16.66 G) of the two ^{31}P atoms ($I = \frac{1}{2}$) (Fig. 4) with the unpaired electron ($S = \frac{1}{2}$). The reported *g* values of close to 2.0 are in good agreement with other reported low spin Fe(I) complexes.[7,22–28] Complex **5a** also shows two distinct carbonyl bands at 1933 cm^{-1} and 1868 cm^{-1} in the ATR-IR spectrum.

The solvothermal reaction of [P(C–Br)P^{O}-iPr] (**1b**) with [$Fe_2(CO)_9$] in either acetonitrile or toluene led to a mixture of several diamagnetic carbonyl containing species. Unfortunately, it was not possible to separate these compounds from each other which prevented their characterization.

In order to determine if the bulkier ligands PCP (P(C–Br)P^{CH_2}-*t*Bu) (**1c**) and (P(C–Br)P^{O}-^{t}Bu) (**1d**) showed any difference in reactivity towards the oxidative addition reaction onto the Fe(0) precursors [$Fe(CO)_5$] and [$Fe_2(CO)_9$], solvothermal reactions were performed in toluene at 120 to 180 °C for 14–24 h. In both cases no formation of an Fe(II) complex was observed. Instead, the moderately air sensitive Fe(I) complexes [Fe(PCP^{CH_2}-*t*Bu)$(CO)_2$] (**5b**) and [Fe(PCP^{O}-*t*Bu)$(CO)_2$] (**5c**) were isolated in yields of 42% and 47%, respectively. Both complexes show two distinct CO bands in the ATR-IR spectrum at 1931 and 1865 cm^{-1} for **5b** and 1947 and 1876 cm^{-1} for **5c**. These complexes exhibit effective magnetic moments of 1.8(3)μ_B (**5b**) and 1.8(1)μ_B (**5c**) respectively, as determined by the Evans NMR method in benzene. These data again are indicative of d^7 low-spin complexes. An overview of the carbonyl stretching frequencies as well as solution magnetic moments of selected Fe(I) pincer complexes are given in Table 1.

Furthermore, X-band EPR studies were conducted with the complexes in toluene glass at 100 K. Analogously to complex

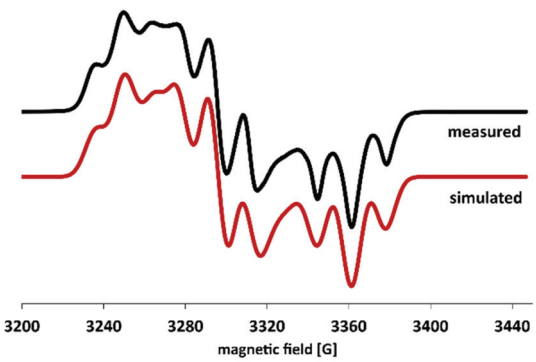

Fig. 4 X-band EPR spectrum of [Fe(PCP^{CH_2}-iPr)$(CO)_2$] (**5a**) in to toluene glass at 100 K at a microwave frequency of 9.86 GHz. The red line represents a simulation with g_x = 2.075 g_y = 2.045 g_z = 2.005, A_x = 14.0 G, A_y = 15.4 G, and A_z = 16.7 G.

This journal is © The Royal Society of Chemistry 2021

5a, these complexes feature rhombic spectra with simulated *g* values of around 2.0, which is close to the *g* value of a free electron (g = 2.002) (see ESI, Fig. S2†) with the anisotropic *g*-factors as well as the hyperfine coupling given in the captions and in Table 2.

The frontier orbitals of complex **5b** are typical of a low spin d^7 species with a square pyramidal geometry (Fig. 5).[12] The spin is located on the metal in the z^2 orbital that is also the single occupied HOMO of the molecules. The other three metal d orbitals, *xz*, *yz* and *xy* are involved in filled molecular orbitals, HOMO−1, HOMO−2 and HOMO−3, respectively. In terms of bonding, the main difference is the donating capability of the PCP ligand. The one with NEt linkers is a stronger donor than the one with CH_2 linkers. This results in an electron richer metal (C(Fe) = −0.19) in the first case (C(Fe) = −0.12 for the molecule with PCP^{CH_2}-*t*Bu). Accordingly, in the PCP^{NEt}-iPr complex the PCP ligand is more positive than the PCP^{CH_2}-*t*Bu ligand in the correspondent molecule (C = 0.24 and 0.17, respectively).[7]

Finally, single crystals of complexes **5b** and **5c** could be grown by cooling saturated solutions in *n*-pentane to −20 °C. Molecular views are presented in Fig. 6 and 7 with selected bond distances and angles reported in the captions. Both com-

Table 1 Carbonyl stretching frequencies and solution magnetic moment of selected Fe(II) pincer complexes

Compound	ν_{CO} [cm^{-1}]	μ_{eff} [μ_B]
$[Fe(PCP^{CH_2}\text{-iPr})(CO)_2]$ (**5a**)	1933, 1868	1.7(8)
$[Fe(PCP^{CH_2}\text{-}t\text{Bu})(CO)_2]$ (**5b**)	1931, 1865	1.8(3)
$[Fe(PCP^{O}\text{-}t\text{Bu})(CO)_2]$ (**5c**)	1947, 1876	1.8(1)
$[Fe(PCP^{NEt}\text{-iPr})(CO)_2]$[7]	1937, 1866	1.8(1)
$[Fe(^{Cy}PNP)(CO)_2]$[22]	1945, 1877	2.0(2)

Table 2 Overview of the simulated anisotropic *g* values and hyperfine coupling constants of complexes **5a–c**

	g values			Hyperfine coupling constants A(^{31}P) [G]		
Compound	g_x	g_y	g_z	A_x	A_y	A_z
$[Fe(PCP^{CH_2}\text{-iPr})(CO)_2]$ (**5a**)	2.075	2.045	2.005	14.0	15.4	16.7
$[Fe(PCP^{CH_2}\text{-}t\text{Bu})(CO)_2]$ (**5b**)	2.051	2.027	2.010	45.0	39.3	48.5
$[Fe(PCP^{O}\text{-}t\text{Bu})(CO)_2]$ (**5c**)	2.044	2.034	1.991	20.3	22.5	14.5

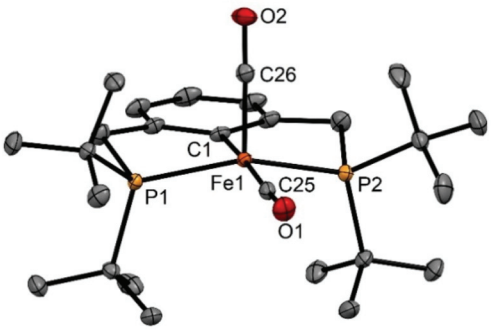

Fig. 6 Crystal structure of $[Fe(PCP^{CH_2}\text{-}t\text{Bu})(CO)_2]$ (**5b**) with 50% thermal ellipsoids (H atoms omitted for clarity). Selected bond lengths (Å) and bond angles (°): Fe1–C1 2.019(1), Fe1–P1 2.2647(4), Fe1–P2 2.2621(4), Fe1–C25 1.781(1), Fe1–C26 1.785(1), C25–Fe1–C26 99.64(5), C1–Fe1–C25 174.01(5,), P1–Fe1–P2 153.24(1).

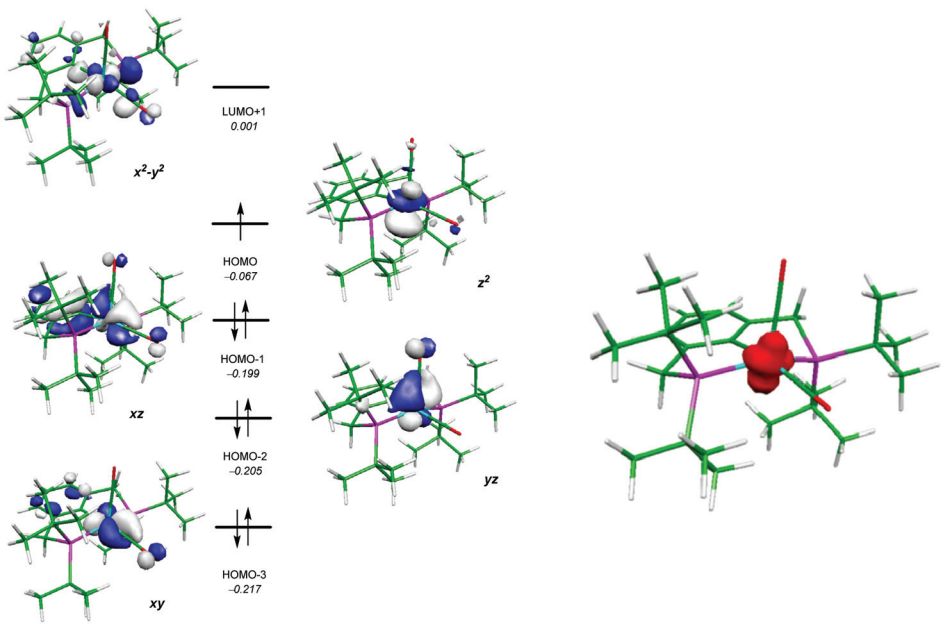

Fig. 5 (left) Frontier orbitals (d-splitting) and (right) spin density of $[Fe(PCP^{CH_2}\text{-}t\text{Bu})(CO)_2]$ (**5b**). Orbital energy values in Hartrees (*italic*).

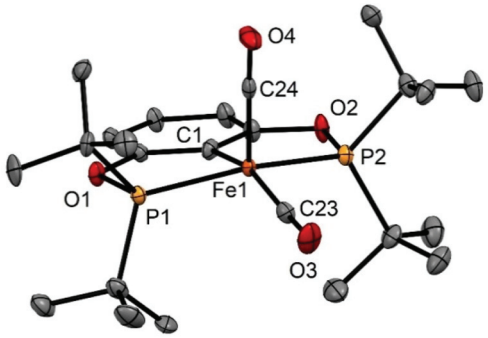

Fig. 7 Crystal structure of [Fe(PCP^{O}-*t*Bu)(CO)$_2$] (**5c**) with 50% thermal ellipsoids (H atoms omitted for clarity). Selected bond lengths (Å) and bond angles (°): Fe1–C1 1.990(4), Fe1–P1 2.238(1), Fe1–P2 2.236(1), Fe1–C24 1.781(4), Fe1–C23 1.795(5), C23–Fe1–C24 92.7(2), C1–Fe1–C23 160.3(2). P1–Fe1–P2 155.46(5).

pounds show a slightly distorted square pyramidal coordination geometry with geometry indices of τ_5 = 0.35 for **5b** and τ_5 = 0.08 for **5c**, respectively. The C_{ipso}–Fe bond lengths are 2.019(1) Å (**5b**) and 1.990(4) (**5c**), respectively.

Conclusion

We describe here the syntheses of various manganese and iron PCP pincer complexes *via* a solvothermal oxidative addition methodology. The PCP pincer ligands consist of a benzene backbone onto which phosphine donors are attached *via* CH_2 or O linkers. Upon reacting [$Mn_2(CO)_{10}$] with the ligands (P(C–Br)P^{CH_2}-iPr) (**1a**) and (P(C–Br)P^{O}-iPr) (**1b**), Mn(I) PCP pincer complexes [Mn(PCP^{CH_2}-iPr)(CO)$_3$] (**2a**) and [Mn(PCP^{O}-iPr)(CO)$_3$] (**2b**) were obtained. This reaction involves a one electron oxidation of the precursor. Protonation of [Mn(PCP^{CH_2}-iPr)(CO)$_3$] (**2a**) with $HBF_4{\cdot}Et_2O$ led to the formation of [Mn(κ^3*P*,*CH*,*P*-P(CH)P^{CH_2}-iPr)(CO)$_3$]BF_4 (**3**) featuring an η^2-C_{aryl}–H agostic bond. The more bulky ligands (P(C–Br)P^{CH_2}-*t*Bu) (**1c**) and (P(C–Br)P^{O}-*t*Bu) (**1d**) did not show any reactivity towards [$Mn_2(CO)_{10}$].

The solvothermal reaction of (P(C–Br)P^{CH_2}-iPr) (**1a**) with [$Fe_2(CO)_9$] afforded the Fe(II) PCP pincer complex [Fe(PCP^{CH_2}-iPr)(CO)$_2$Br] (**4**). Treatment of [Fe(PCP^{CH_2}-iPr)(CO)$_2$Br] (**4**) with Li[HBEt$_3$] afforded the Fe(I) complex [Fe(PCP^{CH_2}-iPr)(CO)$_2$] (**4a**). When using the sterically more demanding ligands (P(C–Br)P^{CH_2}-*t*Bu) (**1c**) and (P(C–Br)P^{O}-*t*Bu)(**1d**) striking differences in reactivity were observed. The reaction of [$Fe_2(CO)_9$] or [$Fe(CO)_5$] led to the formation of the Fe(I) complexes [Fe(PCP^{CH_2}-*t*Bu)(CO)$_2$] (**5b**) and [Fe(PCP^{O}-*t*Bu)(CO)$_2$] (**5c**) rather than complexes of the type [Fe(PCP^{CH_2}-*t*Bu)(CO)$_2$Br].

In sum, the stability of PCP pincer complexes as a function of the linkers follows in general the order NEt (described previously) > CH_2 > O. In particular PCP systems with oxygen linkers appear to be susceptible to hydrolysis resulting in P–O cleavage and decomposition.

Experimental section

General information

All reactions were performed under an inert atmosphere of argon by using Schlenk techniques or in a MBraun inert-gas glovebox. The solvents were purified according to standard procedures.[29] The deuterated solvents were purchased from Aldrich and dried over 3 Å molecular sieves. The ligand precursors P(C–Br)P^{CH_2}-iPr (**1a**),[30] P(C–Br)P^{O}-iPr[10] (**1b**), P(C–Br)P^{O}-*t*Bu (**1c**)[10] were prepared according to the literature. ^{1}H and ^{13}C{^{1}H}, and ^{31}P{^{1}H} NMR spectra were recorded on Bruker AVANCE-250, AVANCE-400, and AVANCE-600 spectrometers. ^{1}H and ^{13}C{^{1}H} NMR spectra were referenced internally to residual protio-solvent, and solvent resonances, respectively, and are reported relative to tetramethylsilane (δ = 0 ppm). ^{31}P{^{1}H} NMR spectra were referenced externally to H_3PO_4 (85%) (δ = 0 ppm).

High resolution-accurate mass data mass spectra were recorded on a hybrid Maxis Qq-aoTOF mass spectrometer (Bruker Daltonics, Bremen, Germany) fitted with an ESI-source. Measured accurate mass data of the [M]$^+$ ions for confirming calculated elemental compositions were typically within ±5 ppm accuracy. The mass calibration was done with a commercial mixture of perfluorinated trialkyl-triazines (ES Tuning Mix, Agilent Technologies, Santa Clara, CA, USA).

CW-EPR spectroscopic measurements were performed on an X-band Bruker Elexsys-II E500 EPR spectrometer (Bruker Biospin GmbH, Rheinstetten, Germany) in solution at 293 K. A high sensitivity cavity (SHQE1119) was used for measurements setting the microwave frequency to 9.86 GHz, the modulation frequency to 100 kHz, the center field to 6000 G, the sweep width to 12 000 G, the sweep time to 30.0 s, the modulation amplitude to 6 G, the microwave power to 15.9 mW, the conversion time to 7.33 ms and the resolution to 4096 points. The spectra were analyzed using the Bruker Xepr software.

(2-Bromo-1,3-phenylene)bis(methylene)bis(di-*t*-butylphosphane) (P(C–Br)P^{CH_2}-*t*Bu) (1d). A solution of the borane di-*tert*-butylphosphine complex (0.98 g, 6.15 mmol) and 2-bromo-1,3-bis(bromomethyl)benzene (1.06 g, 3.10 mmol) in acetone (6 mL) was heated in a sealed microwave glass tube at 80 °C for 18 h. After cooling to room temperature, the solvent was removed under reduced pressure and the formed diphosphonium salt was washed three times with diethyl ether (10 mL). The solid was then dissolved in 30 mL of CH_3OH and 8.5 mL of NEt_3 (61 mmol, 10 equiv.) was added and the solution was stirred for 1 h at 25 °C. After removal of the solvent under reduced pressure, a yellowish residue was obtained which was extracted four times with *n*-pentane (10 mL). The combined extracts were filtered over silica gel and after evaporation of the solvent the product was obtained as colorless solid. Yield: 950 mg (65%). ^{1}H NMR (250 MHz, C_6D_6, δ, 20 °C): 7.68 (d, J = 7.55 Hz, 2 H, C*H*^{4,6}), 7.03 (t, J = 7.58 Hz,1 H, C*H*^{5}), 3.10 (d, J_{HP} = 2.68 Hz, 4H –C*H*$_2$P–), 1.10 (d, J = 10.72 Hz, 36 H, –PC(C*H*$_3$)$_3$). ^{13}C{^{1}H} NMR (63 MHz, δ, C_6D_6, 20 °C) 142.0 (d, J_{CP} = 12.77 Hz, C^{1,3}), 130.1 (dd, J_{CP} = 19.01 Hz, J_{CP} = 2.07 Hz, C^{4,6}), 126.6 (s, C^5), 32.1 (d, J_{CP} = 24.2 Hz, –P*C*(CH$_3$)$_2$), 29.9 (d, J_{CP} =

This journal is © The Royal Society of Chemistry 2021

13.8 Hz, –PC(CH_3)$_2$), 29.7 (d, J_{CP} = 24.5 Hz, –CH_2P–). *Ipso* C not detected. $^{31}P\{^1H\}$ NMR (101 MHz, δ, C_6D_6, 20 °C) 33.6. HRMS (ESI$^+$, CH_3CN/MeOH + 1% H_2O): *m*/*z* calcd for $C_{24}H_{44}BrP_2$ $[M + H]^+$ 473.2096 found 473.2087. Anal. calcd for $C_{24}H_{43}BrP_2$: C, 60.88; H, 9.15. Found: C, 60.65; H, 9.21.

[Mn(PCP^{CH_2}-iPr)(CO)$_3$] (2a). A solution of $[Mn_2(CO)_{10}]$ (46.8 mg, 0.12 mmol) and 2 equiv. of P(C–Br)P^{CH_2}-iPr (**1a**) (100 mg, 0.24 mmol) in CH_3CN (5 mL) in a 20 mL sealed glass tube were stirred for 16 h at 150 °C yielding a clear orange solution. After evaporation of the solvent the orange product was purified by column chromatography (*n*-hexane : EtOAc 10 : 3) and the off-white residue was recrystallized from a solution of *n*-hexane : EtOAc (10 : 1) at −30 °C to yield off-white crystals of **2a** suitable for X-ray diffraction. Yield: 35 mg (31%). ^1H NMR (400 MHz, CD_2Cl_2, δ, 20 °C): 6.99 (d, J = 7.39 Hz, 2H, C$H^{4,6}$), 6.80 (t, J = 7.43 Hz,1H, CH^5), 3.36 (d, J = 7.33 Hz, 4H, CH_2P), 2.37 (m, 4H, –PCH(CH_3)$_2$), 1.28 (dd, J = 13.32 Hz, J = 7.04 Hz,12H, –PCH(CH_3)$_2$), 1.22 (dd, 12H, J = 13.27 Hz, J = 7.18 Hz, –PCH(CH_3)$_2$). $^{13}C\{^1H\}$ NMR (101 MHz, δ, CD_2Cl_2, 20 °C) 226.7 (br, CO), 223.7 (t, J = 23.2 Hz, CO), 173.0 (t, J = 8.2 Hz, *C*–*Mn*), 148.8 (t, J = 9.1 Hz, C^{1,3}), 123.7 (s, C^5), 121.9 (t, J = 6.8 Hz, C^{4,6}), 41.2 (t, J = 10.0 Hz, *C*H$_2$P), 41.0 (t, J = 10.0 Hz, *C*H$_2$P) 28.2 (m, P*C*H(CH_3)$_2$), 26.8 (vt, P*C*H(CH_3)$_2$), 19.4 (d, J = 18.1 Hz, PCH (*C*H$_3$)$_2$). $^{31}P\{^1H\}$ NMR (162 MHz, δ, CD_2Cl_2, 20 °C) 100.3. IR (ATR, ν_{CO}, cm^{-1}) 1985, 1892, 1873. HRMS (ESI$^+$, CH_3CN/MeOH + 1% H_2O): *m*/*z* calcd for $C_{23}H_{36}O_3MnP_2$ $[M + H]^+$ 477.1515 found 477.1516. Anal. calcd for $C_{23}H_{35}O_3MnP_2$: C, 57.98; H, 7.40. Found: C, 58.15; H, 7.49.

[Mn(PCP^O-iPr)(CO)$_3$] (2b). This complex was prepared in analogous fashion to **2a** with **1b** (100 mg, 0.24 mmol) and $[Mn_2(CO)_{10}]$ (46.4 mg, 0.12 mmol) as starting materials. Upon cooling colorless crystals precipitated from the reaction vial. The crystals were washed twice with one mL of cold CH_3CN and dried under vacuum affording the complex as colorless plates. Yield: 45 mg (39%). ^1H NMR (400 MHz, CD_2Cl_2, 20 °C): δ = 6.85 (t, J = 7.8 Hz, 1H, $C_{ar}H$), 6.54 (d, J = 7.8 Hz, 2H, $C_{ar}H$), 2.73 (m, 4H, PCH(CH_3)$_2$), 1.37 (dd, J = 15.3, J = 7.0 Hz 12H, PCH(*C*H$_3$)$_2$), 1.29 (dd, J = 16.0, J = 7.4 Hz 12H, PCH(CH_3)$_2$) ppm; $^{13}C\{^1H\}$ NMR (101 MHz, CD_2Cl_2, 20 °C): δ = 222.1 (br, *C*O), 220.1 (t, *C*O), 165.1 (t, J = 8.6 Hz, C_{ar}C), 135.6 (t, J = 14.3 Hz *C*–*Mn*), 126.5 (C_{ar}H), 105.5 (t, J = 5.1 Hz, C_{ar}H), 32.3 (t, J = 11.0 Hz, P*C*H(CH_3)$_2$), 17.7 (d, J = 18.0 Hz, PCH(*C*H$_3$)$_2$) ppm; $^{31}P\{^1H\}$ NMR (162 MHz, CD_2Cl_2, 20 °C): δ = 220.9 ppm; IR (ATR, ν_{CO}): = 2010, 1921, 1904 cm^{-1}; HRMS (ESI$^+$, CH_3CN/MeOH + 1% H_2O): *m*/*z* calcd for $C_{21}H_{31}O_5NaMnP_2$ ($[M + Na]^+$) 503.0919, found 503.0916. Anal. calcd for $C_{21}H_{31}O_5MnP_2$: C, 52.51; H, 6.50. Found: C, 52.41; H, 6.42.

[Mn((κ^3*P*,*CH*,*P*-P(CH)P^{CH_2}-iPr)(CO)$_3$]BF$_4$ (3). To a solution of [Mn(PCP^{CH_2}-iPr)(CO)$_3$] (**2a**) (7 mg, 14.7 μmol) in CH_2Cl_2 (2 mL), HBF_4·Et_2O (2.5 μL, 17.6 μmol, 1.2 eq.) was added and stirred for 10 min. The solvent was evaporated under reduced pressure and an orange-red solid was obtained which was washed three times with *n*-pentane (1 mL). To remove the excess of HBF_4·Et_2O, the residue was dissolved in CH_2Cl_2 (2 mL) and precipitated upon addition of *n*-pentane (4 mL) yielding **3** as an orange-red solid. Yield: 6 mg (86%). Crystals suitable for X-ray diffraction were obtained by slow evaporation of a concentrated solution of **3** in CH_2Cl_2. ^1H NMR (600 MHz, CD_2Cl_2, δ, 20 °C): 7.70 (t, J = 7.62 Hz, 1H, CH^5), 7.09 (dd, J = 7.30 Hz, J = 2.30 Hz, 2H, C$H^{4,6}$), 4.05 (s, 1H, C*Hipso*), 3.55 (m, 2H, –CH_2P–), 3.08 (m, 2H, –CH_2P–), 2.86 (sep, J = 7.16 Hz 2H, –PCH(CH_3)$_2$), 2.47 (sep, J = 7.42 Hz 2H, –PCH(CH_3)$_2$), 1.46 (m, 6H, –PCH(CH_3)$_2$), 1.35 (m, 18H, –PCH(CH_3)$_2$). $^{13}C\{^1H\}$ NMR (151 MHz, δ, CD_2Cl_2, 20 °C) 226.0 (br, CO), 216.7 (m, CO), 155.6 (s, C^{1,3}), 137.5 (vt, C^5), 126.7 (vt, J = 5.7 Hz, C^{4,6}), 84.3 (t, J = 6.63 Hz, *ipso* C), 33.4 (m, –*C*H$_2$P–), 29.5 (m, –P*C*H(CH_3)$_2$) 26.6 (m, –P*C*H(CH_3)$_2$), 19.0 (m, PCH(*C*H$_3$)$_2$). $^{31}P\{^1H\}$ NMR (243 MHz, δ, CD_2Cl_2, 20 °C) 53.4 (s). IR (ATR, ν_{CO}, cm^{-1}) 2043, 1958, 1911. HRMS (ESI$^+$, CH_3CN/MeOH + 1% H_2O): *m*/*z* calcd for $C_{23}H_{35}O_3MnP_2$ $[M - HBF_4]^+$ 476.1436 found 476.1436. Anal. calcd for $C_{23}H_{36}BF_4O_3MnP_2$: C, 48.96; H, 6.43. Found: C, 48.82; H, 6.50.

[Fe(PCP^{CH_2}-iPr)(CO)$_2$(Br)] (4). A suspension of $[Fe_2(CO)_9]$ (44 mg, 0.12 mmol) and 2 equiv. of **1a** (100 mg, 0.24 mmol) in toluene (5 mL) in a 20 mL sealed glass tube was stirred for 16 h at 140 °C yielding a clear yellow solution. After evaporation of the solvent **4** was obtained as an orange solid which was washed twice with 2 mL of *n*-pentane. Yield: 73 mg (58%). Crystals suitable for X-ray diffraction were obtained by slow diffusion of *n*-pentane in a concentrated solution of **4** in THF. ^1H NMR (600 MHz, C_6D_6, δ, 20 °C): 7.08 (m, 3H, C$H^{4,5,6}$), 3.58 (dt, J = 15.6 Hz, J = 4.6 Hz, 2H, –CH_2P–), 3.19 (dt, J = 15.7 Hz, J = 3.9 Hz, 2H, –CH_2P–), 3.10 (m, 2H, –PCH(CH_3)$_2$), 2.02 (m, 2H, –PCH(CH_3)$_2$), 1.24 (q, J = 7.2 Hz, 6H, –PCH(CH_3)$_2$), 1.08 (q, J = 7.2 Hz, 6H, –PCH(CH_3)$_2$), 1.02 (m, 12H, –PCH(CH_3)$_2$). $^{13}C\{^1H\}$ NMR (151 MHz, δ, C_6D_6, 20 °C) 218.1 (t, J = 25.2 Hz, CO), 213.0 (t, J = 12.7 Hz, CO), 170.6 (t, 12.5 Hz, C–*Fe*), 148.5 (t, J = 8.7 Hz, C^{1,3}), 125.3 (s, C^5), 123.0 (t, J = 7.1 Hz, C^{4,6}), 38.7 (t, J = 14.7 Hz, –*C*H$_2$P–), 26.4 (td, J = 10.1 Hz, J = 4.8 Hz, –P*C*H (CH_3)$_2$), 19.4 (m, PCH(*C*H$_3$)$_2$). $^{31}P\{^1H\}$ NMR (243 MHz, δ, C_6D_6, 20 °C) 88.4 (s). IR (ATR, ν_{CO}, cm^{-1}) 1993, 1938, HRMS (ESI$^+$, CH_3CN/MeOH + 1% H_2O): *m*/*z* calcd for $C_{22}H_{35}O_2FeP_2$ $[M - Br]^+$ 449.1456 found 449.1456. Anal. calcd for $C_{22}H_{35}O_2BrFeP_2$: C, 49.93; H, 6.67. Found: C, 50.04; H, 6.72.

[Fe(PCP^{CH_2}-iPr)(CO)$_2$] (5a). A solution of [Fe(κ^3*P*,*C*,*P*-PCP^{iPr})(CO)$_2$Br] (**4**) (50 mg, 0.094 mmol) in THF (3 mL) was reacted with Li[$HBEt_3$] (60 μL, 1.7 M solution in hexanes, 0.102 mmol) at room temperature. The color of the solution changed immediately from orange to green. After stirring of the solution for 1 h, the solvent was removed under vacuum. The residue was extracted with *n*-pentane (2 mL) and filtered over a syringe filter (polytetrafluoroethylene 0.2 μm). After removal of the solvent under vacuum, **5a** was obtained as green solid. Yield: 36 mg (80%). Crystals suitable for X-ray diffraction were obtained by cooling a saturated solution of **5a** in *n*-pentane to −20 °C. μ_{eff} = 1.7(8)μ_B (Evans method, benzene). IR (ATR, ν_{CO}, cm^{-1}) 1933, 1868. HRMS (ESI$^+$, CH_3CN/MeOH + 1% H_2O): *m*/*z* calcd for $C_{22}H_{35}O_2FeP_2$ $[M]^+$ 449.1456 found 449.1465.

[Fe(PCP^{CH_2}-*t*Bu)(CO)$_2$] (5b). A suspension of $[Fe_2(CO)_9]$ (38.4 mg, 0.11 mmol) and 2 equiv. of **1d** (100 mg, 0.22 mmol) in toluene (5 mL) were placed in a 20 mL sealed glass tube and stirred for 14 h at 120 °C yielding a green solution together

with a brown precipitate. After decantation, the solvent was evaporated *in vacuo* and the green residue was re-dissolved in *n*-pentane (2 mL) and filtered over a syringe filter (polytetrafluoroethylene 0.2 μm). Cooling of the *n*-pentane solution to −20 °C for 48 h afforded green crystals of **5b** suitable for X-ray diffraction. Yield: 45 mg (42%). μ_{eff} = 1.8(3)μ_B (Evans method, benzene). IR (ATR, ν_{CO}, cm^{-1}) 1931, 1865. HRMS (ESI^+, CH_3CN/MeOH + 1% H_2O): *m*/*z* calcd for $C_{26}H_{43}O_2BrP_2$ $[M]^+$ 505.2082 found 505.2075.

[Fe(PCP^O-*t*Bu)(CO)$_2$] (5c). A solution of $[Fe(CO)_5]$ (22 mg, 0.11 mmol) and **1c** (56 mg, 0.12 mmol) in toluene (3 mL) was placed in a 8 mL sealed-glass tube and stirred at 180 °C for 24 h. All volatiles were removed under reduced pressure. The product was extracted with *n*-pentane (2 mL) and after removal of the solvent under vacuum, **5c** was obtained as green solid. Crystals suitable of X-ray diffraction measurement were obtained by cooling a saturated solution of **5c** in *n*-pentane to −20 °C. Yield: 28 mg (47%). μ_{eff} = 1.8(1) (Evans method, benzene). IR (ATR, ν_{CO}, cm^{-1}): 1947, 1876. HRMS (ESI^+, CH_3CN/MeOH + 1% H_2O): *m*/*z* calcd for $C_{23}H_{39}FeO_3P_2$ $[M - CO]^+$ 481.1724 found 481.1713.

X-ray structure determination

X-ray diffraction data of **2a**, **3**, **4**, **5b** and **5c** (CCDC 2097016–2097020†) were collected at T = 100 K in a dry stream of nitrogen on a Bruker Kappa APEX II diffractometer system using graphite-monochromatized Mo-Kα radiation (λ = 0.71073 Å) and fine sliced φ- and ω-scans. Data were reduced to intensity values with SAINT and an absorption correction was applied with the multi-scan approach implemented in SADABS.[31] The structure was solved by the dual-space approach implemented in SHELXT[32] and refined against F^2 with SHELXL.[33] Non-hydrogen atoms were refined with anisotropic displacement parameters. Generally, the H atoms were placed in calculated positions and thereafter refined as riding on the parent C atoms. The agostic H atom in **3** was located from difference Fourier maps and refined freely. The BF_4^- unit was modelled as positionally disordered about two positions with a 91.9 : 8.1(16) ratio. **5c** crystallizes as a five-fold superstructure with very weak superstructure reflections and ten independent molecules in the asymmetric unit (Z' = 10). Residual difference electron density hints towards polytypism: Four Fe atoms were modelled as positionally disordered, which is probably due to an alternative orientation of a distinct layer parallel to (001). Molecular graphics were generated with the program MERCURY.[34]

Computational details

The computational results presented have been achieved in part using the Vienna Scientific Cluster (VSC). Calculations were performed using the GAUSSIAN 09 software package[35] and the B3LYP functional, without symmetry constraints. That functional includes a mixture of Hartree-Fock[36] exchange with DFT[37] exchange–correlation, given by Becke's three parameter functional[38] with the Lee, Yang and Parr correlation functional, which includes both local and non-local terms.[39,40] The basis set used consisted of the Stuttgart/Dresden ECP (SDD) basis set[41] to describe the electrons of Mn and Fe, and a standard 6-31G(d,p) basis set[42] for all other atoms. The frontier orbitals of complex **5b** result from a single point restricted open shell calculation. A Natural Population Analysis (NPA)[43] and the resulting Wiberg indices[44] were used to study the electronic structure and bonding of the optimized species. The NPA analysis was performed with the NBO 5.0 program,[45] and the three-dimensional representations of the orbitals were obtained with Molekel.[46]

Conflicts of interest

There are no conflicts to declare.

Acknowledgements

Financial support by the Austrian Science Fund (FWF) is gratefully acknowledged (Project No. P32570-N). Centro de Química Estrutural acknowledges the financial support of Fundação para a Ciência e Tecnologia (UIDB/00100/2020).

References

1 Coining of the name "pincer": G. van Koten, *Pure Appl. Chem.*, 1989, **61**, 1681–1694.
2 For reviews on pincer complexes, see: (*a*) R. A. Gossage, L. A. van de Kuil and G. van Koten, *Acc. Chem. Res.*, 1998, **31**, 423–431; (*b*) M. Albrecht and G. van Koten, *Angew. Chem., Int. Ed.*, 2001, **40**, 3750–3781; (*c*) M. E. van der Boom and D. Milstein, *Chem. Rev.*, 2003, **103**, 1759–1792; (*d*) J. T. Singleton, *Tetrahedron*, 2003, **59**, 1837–1857; (*e*) L. C. Liang, *Coord. Chem. Rev.*, 2006, **250**, 1152–1177; (*f*) *The Chemistry of Pincer Compounds*, ed. D. Morales-Morales and C. M. Jensen, Elsevier, Amsterdam, 2007; (*g*) H. Nishiyama, *Chem. Soc. Rev.*, 2007, **36**, 1133–1141; (*h*) D. Benito-Garagorri and K. Kirchner, *Acc. Chem. Res.*, 2008, **41**, 201–213; (*i*) J. Choi, A. H. MacArthur, M. Brookhart and A. S. Goldman, *Chem. Rev.*, 2011, **111**, 1761–1779; (*j*) N. Selander and K. J. Szabo, *Chem. Rev.*, 2011, **111**, 2048–2076; (*k*) P. Bhattacharya and H. Guan, *Comments Inorg. Chem.*, 2011, **32**, 88–112; (*l*) S. Schneider, J. Meiners and B. Askevold, *Eur. J. Inorg. Chem.*, 2012, **2012**, 412–429; (*m*) G. van Koten and D. Milstein, Topics in Organometallic Chemistry, in *Organometallic Pincer Chemistry*, Springer, Berlin, 2013, vol. 40; (*n*) K. J. Szabo and O. F. Wendt, *Pincer and Pincer-Type Complexes: Applications in Organic Synthesis and Catalysis*, Wiley-VCH: Weinheim, Germany, 2014; (*o*) M. Asay and D. Morales-Morales, *Dalton Trans.*, 2015, **44**, 17432–17447; (*p*) S. Murugesan and K. Kirchner, *Dalton Trans.*, 2016, **45**, 416–439.
3 C. J. Moulton and B. L. Shaw, *J. Chem. Soc., Dalton Trans.*, 1976, 1020–1024.

 This journal is © The Royal Society of Chemistry 2021

4 (*a*) P. Bhattacharya, J. A. Krause and H. Guan, *Organometallics*, 2011, **30**, 4720–4729; (*b*) P. Bhattacharya, J. A. Krause and H. Guan, *J. Am. Chem. Soc.*, 2014, **136**, 11153–11161; (*c*) P. Bhattacharya, J. A. Krause and H. Guan, *Organometallics*, 2014, **33**, 6113–6121.

5 S. Jiang, S. Quintero-Duque, T. Roisnel, V. Dorcet, S. Sabo-Etienne, C. Darcel and J.-B. Sortais, *Dalton Trans.*, 2016, **45**, 11101–11108.

6 A. Dauth, U. Gellrich, Y. Diskin-Posner, Y. Ben-David and D. Milstein, *J. Am. Chem. Soc.*, 2017, **139**, 2799–2807.

7 D. Himmelbauer, M. Mastalir, B. Stöger, L. F. Veiros, M. Pignitter, V. Somoza and K. Kirchner, *Inorg. Chem.*, 2018, **57**, 7925–7931.

8 D. Himmelbauer, B. Stöger, L. F. Veiros and K. Kirchner, *Organometallics*, 2018, **37**, 3475–3479.

9 D. Himmelbauer, M. Mastalir, B. Stöger, L. F. Veiros and K. Kirchner, *Organometallics*, 2018, **37**, 3631–3638.

10 D. Himmelbauer, B. Stöger, L. F. Veiros, M. Pignitter and K. Kirchner, *Organometallics*, 2019, **38**, 4669–4678.

11 W. Eder, B. Stöger and K. Kirchner, *Monatsh. Chem.*, 2019, **150**, 1235–1240.

12 S. Murugesan, B. Stöger, E. Pittenauer, G. Allmaier, L. F. Veiros and K. Kirchner, *Angew. Chem., Int. Ed.*, 2016, **55**, 3045–3048.

13 S. R. M. M. de Aguiar, B. Stöger, E. Pittenauer, G. Allmaier, L. F. Veiros and K. Kirchner, *Organometallics*, 2016, **35**, 3032–3039.

14 (*a*) A. Vigalok, O. Uzan, L. J. W. Shimon, Y. Ben-David, J. M. L. Martin and D. Milstein, *J. Am. Chem. Soc.*, 1998, **120**, 12539–12544; (*b*) A. Vigalok, B. Rybtchinski, L. J. W. Shimon, Y. Ben-David and D. Milstein, *Organometallics*, 1999, **18**, 895–905; (*c*) M. Montag, L. Schwartsburd, R. Cohen, G. Leitus, Y. Ben-David, J. M. L. Martin and D. Milstein, *Angew. Chem., Int. Ed.*, 2007, **46**, 1901–1904; (*d*) C. M. Frech, L. J. W. Shimon and D. Milstein, *Organometallics*, 2009, **28**, 1900–1908; (*e*) M. Montag, I. Efremenko, R. Cohen, L. J. W. Shimon, G. Leitus, Y. Diskin-Poser, Y. Ben-David, H. Salem, J. M. L. Martin and D. Milstein, *Chem. – Eur. J.*, 2010, **16**, 328–353.

15 A. C. Albeniz, G. Schulte and R. H. Crabtree, *Organometallics*, 1992, **11**, 242–249.

16 (*a*) P. Dani, T. Karlen, R. A. Gossage, W. J. J. Smeets, A. L. Spek and G. van Koten, *J. Am. Chem. Soc.*, 1997, 11317–11318; (*b*) P. Dani, M. A. M. Toorneman, G. P. M. van Klink and G. van Koten, *Organometallics*, 2000, **19**, 5287–5296.

17 M. A. McLoughlin, R. J. Flesher, W. C. Kaska and H. A. Mayer, *Organometallics*, 1994, **13**, 3816–3822.

18 M. E. van der Boom, M. A. Iron, O. Atasoylu, L. J. W. Shimon, H. Rozenberg, Y. Ben-David, L. Konstantinovski, J. M. L. Martin and D. Milstein, *Inorg. Chem. Acta*, 2004, **357**, 1854–1864.

19 D. G. Gusev, M. Madott, F. M. Dolgushin, K. A. Lyssenko and M. Y. Antipin, *Organometallics*, 2000, **19**, 1734–1739.

20 C. Barthes, C. Lepetit, Y. Canac, C. Duhayon, D. Zargarian and R. Chauvin, *Inorg. Chem.*, 2013, **52**, 48–58.

21 S. D. T. Cherry, W. Kaminsky and D. M. Heinekey, *Organometallics*, 2016, **35**, 2165–2169.

22 C. V. Thompson, H. D. Arman and Z. J. Tonzetich, *Organometallics*, 2017, **36**, 1795–1802.

23 N. Ehrlich, M. Kreye, D. Baabe, P. Schweyen, M. Freytag, P. G. Jones and M. D. Walter, *Inorg. Chem.*, 2017, **56**, 8415–8422.

24 A. M. Tondreau, C. Milsmann, E. Lobkovsky and P. J. Chirik, *Inorg. Chem.*, 2011, **50**, 9888–9895.

25 J. Pecak, B. Stöger, M. Mastalir, L. F. Veiros, L. P. Ferreira, M. Pignitter, W. Linert and K. Kirchner, *Inorg. Chem.*, 2019, **58**, 4641–4646.

26 M. Glatz, B. Stöger, B. Bichler, G. Bauer, L. F. Veiros, M. Pignitter and K. Kirchner, *Eur. J. Inorg. Chem.*, 2020, 1101–1105.

27 C. Kupper, A. Schober, S. Demeshko, M. Bergner and F. Meyer, *Inorg. Chem.*, 2015, **54**, 3096–3098.

28 S. Kuriyama, K. Arashiba, K. Nakajima, Y. Matsuo, H. Tanaka, K. Ishii, K. Yoshizawa and Y. Nishibayashi, *Nat. Commun.*, 2016, **7**, 12181.

29 W. L. Armarego, *Purification, of laboratory chemicals*, Butterworth-Heinemann, 2017.

30 B. Rybtchinski, Y. Ben-David and D. Milstein, *Organometallics*, 1997, **16**, 3786–3793.

31 *Bruker computer programs: APEX3, SAINT and SADABS*, Bruker AXS Inc., Madison, WI, 2020.

32 G. M. Sheldrick, *Acta Crystallogr., Sect. A: Found. Adv.*, 2015, **A71**, 3–8.

33 G. M. Sheldrick, *Acta Crystallogr., Sect. C: Struct. Chem.*, 2015, **C71**, 3–8.

34 C. F. Macrae, P. R. Edgington, P. McCabe, E. Pidcock, G. P. Shields, R. Taylor, M. Towler and J. van de Streek, *J. Appl. Crystallogr.*, 2006, **39**, 453–457.

35 M. J. Frisch, G. W. Trucks, H. B. Schlegel, G. E. Scuseria, M. A. Robb, J. R. Cheeseman, G. Scalmani, V. Barone, B. Mennucci, G. A. Petersson, H. Nakatsuji, M. Caricato, X. Li, H. P. Hratchian, A. F. Izmaylov, J. Bloino, G. Zheng, J. L. Sonnenberg, M. Hada, M. Ehara, K. Toyota, R. Fukuda, J. Hasegawa, M. Ishida, T. Nakajima, Y. Honda, O. Kitao, H. Nakai, T. Vreven, J. A. Montgomery Jr., J. E. Peralta, F. Ogliaro, M. Bearpark, J. J. Heyd, E. Brothers, K. N. Kudin, V. N. Staroverov, R. Kobayashi, J. Normand, K. Raghavachari, A. Rendell, J. C. Burant, S. S. Iyengar, J. Tomasi, M. Cossi, N. Rega, J. M. Millam, M. Klene, J. E. Knox, J. B. Cross, V. Bakken, C. Adamo, J. Jaramillo, R. Gomperts, R. E. Stratmann, O. Yazyev, A. J. Austin, R. Cammi, C. Pomelli, J. W. Ochterski, R. L. Martin, K. Morokuma, V. G. Zakrzewski, G. A. Voth, P. Salvador, J. J. Dannenberg, S. Dapprich, A. D. Daniels, Ö. Farkas, J. B. Foresman, J. V. Ortiz, J. Cioslowski and D. J. Fox, *Gaussian 09, Revision A.02*, Gaussian, Inc., Wallingford CT, 2009.

36 W. J. Hehre, L. Radom, P. v. R. Schleyer and J. A. Pople, *Ab Initio Molecular Orbital Theory*, John Wiley & Sons, NY, 1986.

37 R. G. Parr and W. Yang, *Density Functional Theory of Atoms and Molecules*, Oxford University Press, New York, 1989.

38 A. D. Becke, *J. Chem. Phys.*, 1993, **98**, 5648–5652.
39 C. Lee, W. Yang and R. G. Parr, *Phys. Rev. B: Condens. Matter Mater. Phys.*, 1988, **37**, 785–789.
40 B. Miehlich, A. Savin, H. Stoll and H. Preuss, *Chem. Phys. Lett.*, 1989, **157**, 200–206.
41 (*a*) U. Haeusermann, M. Dolg, H. Stoll, H. Preuss, P. Schwerdtfeger and R. M. Pitzer, *Mol. Phys.*, 1993, **78**, 1211–1224; (*b*) W. Kuechle, M. Dolg, H. Stoll and H. Preuss, *J. Chem. Phys.*, 1994, **100**, 7535–7542; (*c*) T. Leininger, A. Nicklass, H. Stoll, M. Dolg and P. Schwerdtfeger, *J. Chem. Phys.*, 1996, **105**, 1052–1059.
42 (*a*) R. Ditchfield, W. J. Hehre and J. A. Pople, *J. Chem. Phys.*, 1971, **54**, 724–728; (*b*) W. J. Hehre, R. Ditchfield and J. A. Pople, *J. Chem. Phys.*, 1972, **56**, 2257–2261; (*c*) P. C. Hariharan and J. A. Pople, *Mol. Phys.*, 1974, **27**, 209–214; (*d*) M. S. Gordon, *Chem. Phys. Lett.*, 1980, **76**, 163–168; (*e*) P. C. Hariharan and J. A. Pople, *Theor. Chim. Acta*, 1973, **28**, 213–222.
43 (*a*) J. E. Carpenter and F. Weinhold, *J. Mol. Struct.*, 1988, **169**, 41–62; (*b*) J. E. Carpenter, PhD. Thesis, University of Wisconsin, Madison, WI, 1987; (*c*) J. P. Foster and F. Weinhold, *J. Am. Chem. Soc.*, 1980, **102**, 7211–7218; (*d*) A. E. Reed and F. Weinhold, *J. Chem. Phys.*, 1983, **78**, 4066–4073; (*e*) A. E. Reed and F. Weinhold, *J. Chem. Phys.*, 1985, **83**, 1736–1740; (*f*) A. E. Reed, R. B. Weinstock and F. Weinhold, *J. Chem. Phys.*, 1985, **83**, 735–746; (*g*) A. E. Reed, L. A. Curtiss and F. Weinhold, *Chem. Rev.*, 1988, **88**, 899–926; (*h*) F. Weinhold and J. E. Carpenter, *The Structure of Small Molecules and Ions*, Plenum, New York, 1988, p. 227.
44 (*a*) K. B. Wiberg, *Tetrahedron*, 1968, **24**, 1083–1096; (*b*) Wiberg indices are electronic parameters related with the electron density in between two atoms, which scale as bond strength indicators. They can be obtained from a Natural Population Analysis.
45 E. D. Glendening, J. K. Badenhoop, A. E. Reed, J. E. Carpenter, J. A. Bohmann, C. M. Morales and F. Weinhold, *NBO 5.0, Theoretical Chemistry Institute*, University of Wisconsin, Madison, 2001.
46 S. Portmann and H. P. Lüthi, *Chimia*, 2000, **54**, 766–770.

This journal is © The Royal Society of Chemistry 2021